Translational Oncology 16 (2022) 101307

Contents lists available at ScienceDirect

Translational Oncology

journal homepage: www.elsevier.com/locate/tranon

Original Research

Targeting AURKA in treatment of peritoneal tumor dissemination in gastrointestinal cancer

Hiroki Ozawa [a,b], Hiroshi Imazeki [a], Yamato Ogiwara [a], Hirofumi Kawakubo [b], Kazumasa Fukuda [b], Yuko Kitagawa [b], Chie Kudo-Saito [a,*]

[a] Department of Immune Medicine, National Cancer Center Research Institute, 5-1-1 Tsukiji, Chuo-ku, Tokyo 104-0045, Japan
[b] Department of Surgery, Keio University School of Medicine, Tokyo 160-8582, Japan

ARTICLE INFO

Keywords:
Gastric cancer
Ascites
Peritoneal metastasis
Treatment resistance
Immune checkpoint
Polyploidy

ABSTRACT

Intraperitoneal (i.p.) tumor dissemination and the consequent malignant ascites remain unpredictable and incurable in patients with gastrointestinal (GI) cancer, and practical advances in diagnosis and treatment are urgently needed in the clinical settings. Here, we explored tumor biological and immunological mechanisms underlying the i.p. tumor progression for establishing more effective treatments.

We established mouse tumor ascites models that murine and human colorectal cancer cells were both i.p. and subcutaneously (s.c.) implanted in mice, and analyzed peritoneal exudate cells (PECs) obtained from the mice. We then evaluated anti-tumor efficacy of agents targeting the identified molecular mechanisms using the ascites models. Furthermore, we validated the clinical relevancy of the findings using peritoneal lavage fluids obtained from gastric cancer patients.

I.p. tumor cells were giant with large nuclei, and highly express AURKA, but less phosphorylated TP53, as compared to s.c. tumor cells, suggesting polyploidy-like cells. The i.p. tumors impaired phagocytic activity and the consequent T-cell stimulatory activity of $CD11b^{+}Gr1^{+}PD1^{+}$ myeloid cells by GDF15 that is regulated by AURKA, leading to treatment resistance. Blocking AURKA with MLN8237 or siRNAs, however, abrogated the adverse events, and induced potent anti-tumor immunity in the ascites models. This treatment synergized with anti-PD1 therapy. The $CD11b^{+}PD1^{+}$ TAMs are also markedly expanded in the PECs of gastric cancer patients.

These suggest AURKA is a determinant of treatment resistance of the i.p. tumors. Targeting the AURKA-GDF15 axis could be a promising strategy for improving clinical outcome in the treatment of GI cancer.

Introduction

Peritoneal tumor dissemination is frequently seen in gastrointestinal (GI) cancer, and leads to malignant ascites that suddenly and repeatedly relapses even after being drained from the peritoneal cavity, resulting in poor prognosis [1,2]. The therapeutic options are extremely limited to palliative treatments of the symptoms, despite many clinical trials using inventive methods, such as cytoreductive surgery and hyperthermic intraperitoneal (i.p.) chemotherapy [3,4]. Advances in molecular profiling of the i.p. tumors obtained from mouse tumor models and cancer patients have revealed the landscape, and epithelial-to-mesenchymal transition (EMT) has been considered as a key program of tumor dissemination [5,6]. Many agents targeting the molecular pathways have been clinically developed [7,8], while the evaluation is still underway.

Accumulating evidence shows that tumor cells evolve intrinsically and extrinsically through interplay with numerous components in the host [8]. Macrophages that produce various pro-inflammatory and angiogenic cytokines are considered as a prominent villain to facilitate i.p. tumor progression [9]. Chronic inflammation causes exhaustion and dysfunction of anti-tumor effector cells by inducing multiple immune checkpoint (IC) molecules, including CTLA4, PD1, LAG3, and TIGIT [10,11]. However, clinical outcome of the anti-PD1/PDL1 therapy is still low, and the therapeutic efficacy on i.p. tumors remains unclear [12,13]. Several biomarkers, including PDL1 expression, high microsatellite instability, and mismatch repair deficiency, have been identified, while these are not necessarily correlated with the clinical outcomes [12,13]. Thus, more effective biomarkers and treatments are urgently needed for prediction and prevention of onset and progression of i.p. tumors in clinical settings. In this study, we attempted to identify tumor biological

* Corresponding author.
E-mail address: ckudo@ncc.go.jp (C. Kudo-Saito).

https://doi.org/10.1016/j.tranon.2021.101307
Received 20 September 2021; Received in revised form 1 November 2021; Accepted 30 November 2021
Available online 10 December 2021

and immunological components to produce refractory i.p. tumors using mouse tumor ascites models and peritoneal lavage fluids obtained from gastric cancer patients.

Materials and methods

Cell lines and mice

Murine colorectal cancer (CRC) Colon26 cells were purchased from Cell Resource Center for Biomedical Research at Tohoku University in Japan, and MC38 cells were kindly provided by the NCI at the NIH in USA. Human CRC HCT116 cells were purchased from the ATCC. The cells were authenticated by short tandem repeat profiling, and were tested for Mycoplasma negativity using a Hoechst-staining detection kit (MP Biomedicals) before use. The cells were expanded in 10% FBS-containing DMEM (GIBCO) at 37 °C, and were frozen in liquid nitrogen to avoid changes occurred by the long-term culture until use. The cells were trypsinized and washed in MEMα (Wako) before use for experiment. Five-week-old female BALB/c, C57BL/6, and BALB/c-nu nude mice were purchased from Charles River Laboratories in Japan, and were maintained under pathogen-free conditions. The mice were used according to the protocol approved by the Animal Care and Use Committee at the National Cancer Center Research Institute in Japan.

In vivo therapy

We established mouse tumor ascites models by subcutaneously (s.c.; 5×10^5) and intraperitoneally (i.p.; 2×10^5) implanting with Colon26 cells to observe both solid and i.p. tumors simultaneously. Treatments with agents were started on day 3–5 after tumor implantation. The following agents were used: Anti-PD1 mAb (Clone 29F.1A12; BioLegend), anti-LAG3 mAb (Clone C9B7W; BioXCell), anti-TIGIT mAb (Clone 1G9; BioXCell), mouse IgG (mIgG, Clone MOPC-21; BioXCell), an AURKA inhibitor MLN8237 (Selleck), a CDK4/6 inhibitor PD0332991 (AdooQ), and 5-fluorouracil (5-Fu; Wako). To deplete $CD8^+$ T cells and NK cells, mice were i.p. injected with anti-CD8 mAb (Clone 2.43, 200 μg; BioXCell) or anti-asialo GM1 polyclonal Ab (20 μL; BioLegend) before and during the treatments. The depletion efficacy (> 80%) was validated by flow cytometry. Tumor size was measured (0.5 x Length x $Width^2$, mm^3), and mouse survival was observed. Two weeks after tumor implantation, s.c. tumors, spleens and peritoneal exudate cells (PECs) were harvested from the mice for assays. Splenic $CD8^+$ T cells (2×10^5) were stimulated with the $H\text{-}2L^d$-restricted tumor antigen AH1 peptides (MBL), and were tested for cytotoxic activity (target = Colon26, 4 h) as described before [14]. Cytotoxic activity of NK cells was similarly assessed using Yac-1 cells as a target.

Characterization of peritoneal macrophages

Two weeks after tumor implantation, $CD11b^+$ cells were sorted from the PECs using a BD IMag system with magnetic particle-conjugated anti-mouse CD11b mAb, and were cultured in 10% FBS/RPMI1640 (GIBCO) for 2 h to isolate adhered cells as tumor-associated macrophages (TAMs). In phagocytosis assay, PKH26-labeled TAMs (1×10^5) were cocultured with CFSE-labeled tumor cells (1×10^5) for 2 h, and were analyzed by flow cytometry. The TAMs (MMC inactivation) were cocultured with splenic $CD3^+$ T cells, or were s.c. coinjected with tumor cells (1:1) in mice.

Characterization of tumor cells

Tumor cells transfected with the plasmid vector pcDNA3.1(+) (Invitrogen) were used. Two weeks after implantation, tumor cells were isolated from s.c. tumors or PECs, and were cultured with Geneticin (Merck)-containing 10%FCS/DMEM (GIBCO). Gene knockdown was conducted using the specific siRNAs, and the transfection efficacy was validated by RT-PCR, flow cytometry, or ELISA, and one siRNA having the highest knockdown efficiency was mainly used in assays as described before [14]. Tumor-cultured supernatant fluids (1×10^5 cells/10 ml/3 days) were tested for IL33 (R&D) or GDF15 (R&D) using ELISA kits, and were used to stimulate the $CD11b^+$ PECs or CTLs for 3 days. Tumor-antigen SAGE-specific CTLs were established as described before [14]. GDF15 (20 ng/ml; R&D) was used as a control. Tumor cells (5×10^3 cells/well) were cultured with agents for 2 days, and the proliferation was assessed by WST1 assay (Takara). Graphs were depicted as the percentage of the control without agents (100%). In the *in vivo* setting, tumor cells (5×10^5) were s.c. implanted in mice, and the mice were treated with agents.

Flow cytometric analysis

After Fc blocking, cells were stained with the following immunofluorescence-conjugated antibodies: Anti-mouse CD3e-FITC (BD Biosciences), anti-mouse CD3e-APC (BD), anti-mouse CD8a-PE or -PE-Cy5 (BioLegend), anti-mouse CD11b-FITC or -PE (BioLegend), anti-mouse CD45-PE-Cy5 (BD), anti-mouse Gr1-PE (BD), anti-mouse DX5-PE (BD), anti-mouse PD1-FITC (BioLegend), anti-mouse CTLA4-PE (BioLegend), anti-mouse LAG3-FITC (BioLegend), anti-mouse TIGIT-PE (BioLegend), anti-mouse/human AURKA (Abcam), anti-mouse/human pTP53-FITC (CST), anti-mouse GDF15 (R&D Systems), anti-human CD3-BUV496 (BD), anti-human CD4-PerCP-Cy5.5 (BioLegend), anti-human CD8-BUV395 (BD), anti-human CD56- BUV650 (BioLegend), anti-human CD11b-BV510 (BioLegend), anti-human CD45-APC-Cy7 (BioLegend), anti-human PD1-BV605 (BioLegend), anti-human EOMES-APC (R&D), anti-human LAG3-BV650 (BioLegend), anti-human TIGIT-PE-Cy7 (BioLegend), anti-human PDL1-FITC (BD), anti-human CD155-PerCP-Cy5.5 (BioLegend), anti-human ST2-FITC (MBL), or the appropriate isotype control. For intracellular staining, cells were treated with Cytofix/Cytoperm solution (BD) before the staining. In mouse study, data were acquired using the FACSCalibur cytometer (BD), and were analyzed by Cellquest software (BD). In clinical study, data were acquired using a BD LSR Fortessa X-20 cytometer (BD), and were analyzed by FlowJo software (BD). Before defining the specific molecular expressions, debris was firstly excluded by FSC/SSC followed by gating $CD45^+$ leukocytes, and immunofluorescence intensity was compared to the isotype control.

Clinical analysis of human PECs

Gastric cancer patients were registered at Keio University Hospital after obtaining informed consent (July 2018–March 2020; Table S1). The peritoneal cavity was washed with 300 ml saline, and the lavage fluids were collected at initiation of surgical tumor resection according to the protocol (#20,180,064) approved by the Institutional Review Board of the Keio University School of Medicine. Informed consent was obtained from all subjects. All activities were conducted in accordance with the ethical principles of the Declaration of Helsinki. PECs derived from the lavage fluids were analyzed by flow cytometry.

Statistical analysis

Data are shown as means ± SDs unless otherwise specified. Significant differences (P value < 0.05) were evaluated using GraphPad Prism 7 software (MDF). Two groups were compared by the unpaired two-tailed Student's t-test. Multiple groups were compared by one-way ANOVA, followed by the Bonferroni post-hoc test for pairwise comparison of groups on the basis of the normal distributions. Non-parametric groups were analyzed by the Mann-Whitney test. In the combination therapy, significance to the single treatment was evaluated using a two-way ANOVA with Bonferroni post-hoc test. Mouse survival was analyzed by Kaplan-Meier method and ranked according to the Mantel-Cox log-rank test. Correlation between two factors in clinical study was

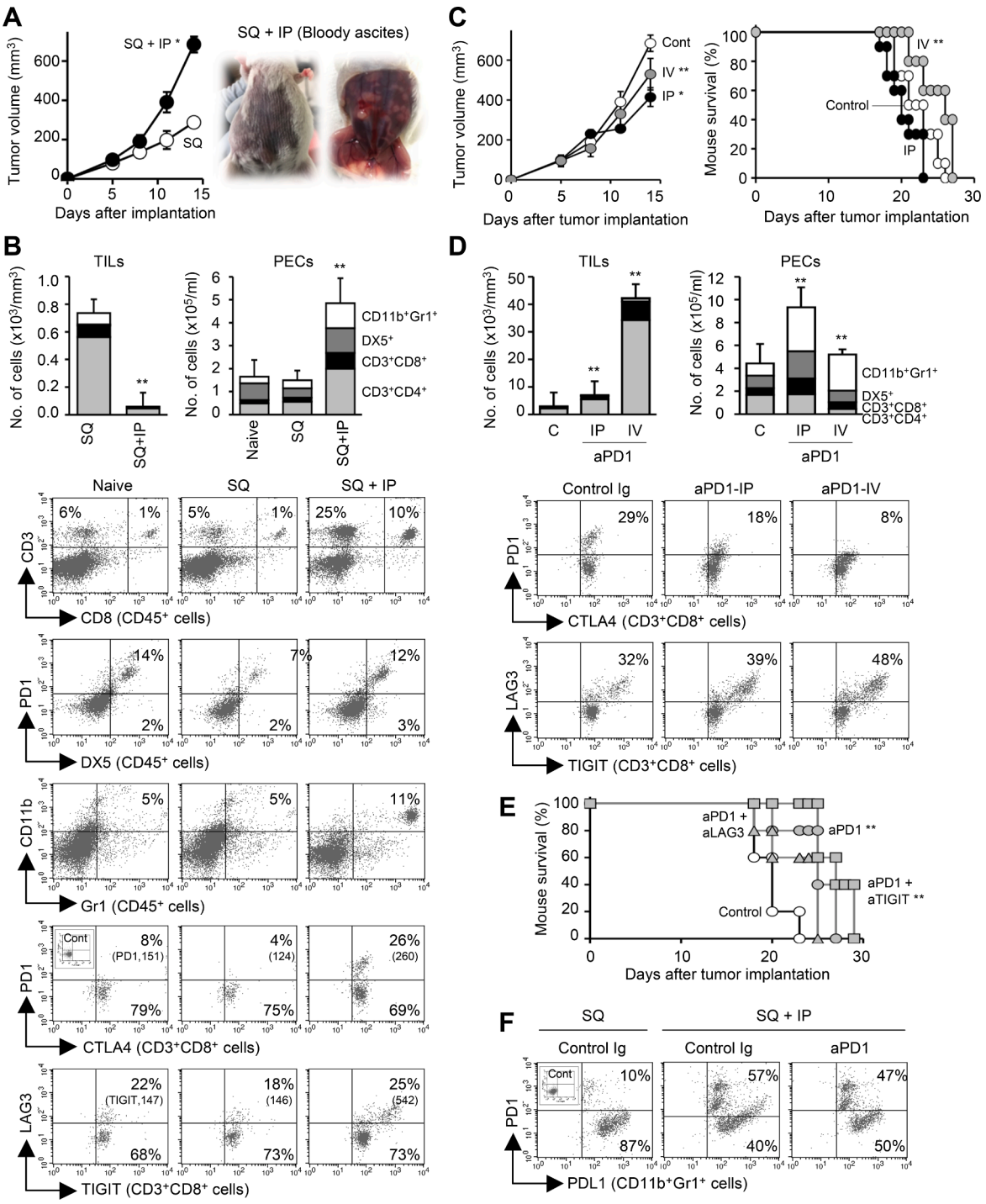

Fig. 1. Anti-PD1 therapy is ineffective in mouse tumor ascites models. (A, B) Establishment of mouse tumor ascites models. BALB/c mice were subcutaneously (s.c./SQ, 5×10^5 cells) and/or intraperitoneally (i.p./IP, 2×10^5 cells) implanted with murine colorectal cancer Colon26 cells ($n = 5$). Tumor growth was measured (A), and s.c. tumor-infiltrating cells (TILs) and peritoneal exudate cells (PECs) were analyzed by flow cytometry on day 14 after tumor implantation (B). Mean of fluorescence intensity (MFI) of PD1 or TIGIT is indicated in a bracket. $^*P < 0.01$, $^{**}P < 0.05$ versus SQ. (C, D) Anti-PD1 therapeutic efficacy in the ascites models. The tumor ascites models were i.p. or intravenously (i.v./IV) injected with anti-PD1 mAb or mouse IgG (mIgG) as a control (10 mg/kg) on days 5 and 9 after tumor implantation ($n = 10$). The therapeutic efficacies on tumor growth and mouse survival were evaluated (C), and TILs and PECs were analyzed by flow cytometry on day 14 (D). $^*P < 0.01$, $^{**}P < 0.05$ versus control. (E) No contribution of blocking other immune checkpoint pathways to the anti-PD1 therapy ($n = 5$). Open circles, control mIgG. Gray circles, anti-PD1 mAb. Gray triangles, anti-PD1 mAb + anti-LAG3 mAb. Gray squares, anti-PD1 mAb + anti-TIGIT mAb. $^{**}P < 0.05$ versus control. (F) Expansion of a $PD1^+PDL1^+$ subset in the $CD11b^+Gr1^+$ PECs of the ascites models. The inset dot plot shows $CD11b^+Gr1^+$ PECs stained with isotype control. In the stacked bar graphs, light gray, $CD3^+CD4^+$ T cells; closed, $CD3^+CD8^+$ T cells; dark gray, $DX5^+$ NK cells; and open, $CD11b^+Gr1^+$ myeloid cells. Graphs show means ± SDs. Representative data of five independent experiments.

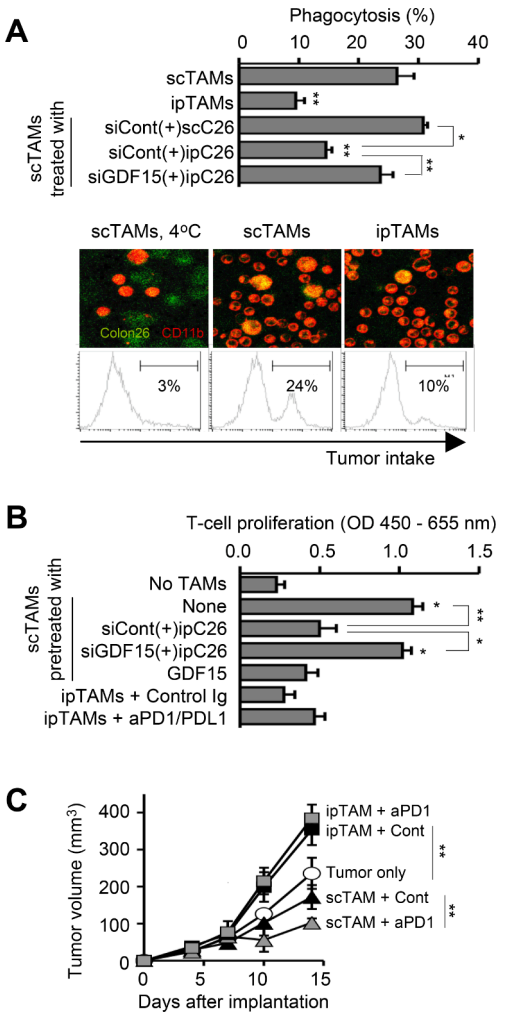

Fig. 2. Peritoneal macrophages create anti-PD1 resistance. (A) Phagocytic activity of the CD11b$^+$ PECs is impaired by i.p. tumors. Adherent CD11b$^+$ cells were sorted from the PECs of the ascites models (ipTAMs) or s.c. implanted solid tumor models (scTAMs) 2 weeks after tumor implantation, and the scTAMs were stimulated with tumor supernatants (5 x dilution) for 3 days. Tumor cells were isolated from the s.c. tumor tissues (scC26) or PECs (ipC26) 2 weeks after tumor implantation, and the 3-day-cultured supernatants were used for the stimulation. The CD11b$^+$ PECs (PKH26, red) were cocultured (1:1) with Colon26 cells (CFSE, green) for 2 h, and were analyzed for tumor-engulfing TAMs by flow cytometry (n = 3). (B) T-cell stimulatory activity of the CD11b$^+$ PECs is impaired by i.p. tumors. Splenic CD3$^+$ T cells were cocultured with the CD11b$^+$ PECs (pretreated with tumor supernatants or GDF15 at 20 ng/ml for 3 days) in the presence of anti-CD3 mAb (1 μg/ml) and/or anti-PD1/PDL1 mAbs (5 μg/ml) for 3 days (n = 3). (C) The ipTAMs promote *in vivo* tumor progression leading to anti-PD1 resistance. Tumor cells were s.c. coinjected (1:1) with the scTAMs (triangles) or ipTAMs (squares), and the mice were treated with anti-PD1 mAb (gray) or mIgG (closed) on days 4 and 7 after implantation (n = 5). Open circles, tumor only. Graphs show means ± SDs. *P < 0.01, **P < 0.05 versus control. Representative data of three independent experiments.

evaluated by the nonparametric Spearman's rank test.

Results

Anti-PD1 therapy is ineffective in mouse tumor ascites models

To established mouse tumor ascites models, we used murine CRC Colon26 cells, because mouse gastric cancer cell lines were unavailable to us. Mimicking GI cancer patients with malignant ascites, Colon26 cells were s.c. and i.p. implanted in BALB/c mice to observe progression of both solid tumors and hemorrhagic tumor ascites simultaneously (Fig. 1A). In the ascites models, s.c. tumor growth was aggressively promoted (P = 0.0002; Fig. 1A), and immune cells rarely infiltrated in there (Fig. 1B). In contrast, immune cells massively increased in the peritoneal cavity, and CD3$^+$CD8$^+$ T cells in the peritoneal exudate cells (PECs) highly expressed multiple IC molecules (Fig. 1B), implying exhausted status [10,11]. We then treated the ascites models with anti-PD1 mAb by two different routes, i.p. or i.v., on days 5 and 9 after tumor implantation. The i.v. treatment, but not i.p. treatment, showed statistically significant anti-tumor effects on both s.c. tumor growth (P = 0.046) and mouse survival (P = 0.032) as compared to the control group (Fig. 1C). However, the impact of the therapeutic efficacy was small as all mice died within 30 days after implantation. In the i.v. treated mice, CD4$^+$ and CD8$^+$ T cells abundantly increased within the s.c. tumors (P = 0.015 versus i.p. treatment), and CD3$^+$CD8$^+$PD1$^+$CTLA4$^+$ cells clearly decreased in the PECs (Fig. 1D). However, CD3$^+$CD8$^+$LAG3$^+$TIGIT$^+$ cells were rather expanded in the PECs (Fig. 1D). We then combined anti-LAG3 or anti-TIGIT therapy with the anti-PD1 therapy. However, the anti-PD1 therapeutic efficacy was not synergistically enhanced by either therapy (Fig. 1E). Interestingly, a PD1$^+$ subset was dramatically expanded in the CD11b$^+$Gr1$^+$PDL1$^+$ myeloid cells in the PECs of the ascites models (Fig. 1F).

Peritoneal macrophages create anti-PD1 resistance

We then characterized adherent CD11b$^+$ cells isolated from PECs of the ascites models (designated ipTAMs) or the solid tumor models (designated scTAMs). The ipTAMs engulfed much less tumor cells than the scTAMs (P = 0.017; Fig. 2A), and were unable to stimulate T-cell proliferation, although the scTAMs enhanced it as antigen-presenting cells (APCs; Fig. 2B). This event was not rescued by blocking PD1/PDL1. These suggest the ipTAMs are dysfunctional APCs, and the PD1-PDL1 axis is not involved in this mechanism (Fig. 2B). When tumor cells were s.c. coinjection with the ipTAMs, tumor growth was aggressively enhanced as compared to the control without TAMs (P = 0.028), and this was not interfered by anti-PD1 treatment (Fig. 2C). These suggest the ipTAMs also directly promote tumor progression, and anti-PD1 therapy is ineffective in suppressing the ipTAM-caused tumor progression. When the scTAMs were stimulated with supernatants of tumor cells isolated from PECs (designated ipC26), but not tumor cells isolated from s.c. tumors (designated scC26) of the ascites models, the phagocytic activity (P = 0.030; Fig. 2A) and the T-cell stimulatory activity (P = 0.022; Fig. 2B) were significantly reduced. This suggests i.p. tumors impair TAM functions.

AURKA is a determinant of chemoresistance of the i.p. tumor cells

We then compared between the ipC26 and scC26 cells. The proliferative ability and sensitivity to 5-fluorouracil (5-Fu) of the ipC26 cells were significantly lower than those of the scC26 cells (P < 0.0001; Fig. 3A and B). The ipC26 cells were giant having large nuclei (Fig. 3A), just like polyploidy that is known as a cancer stemness for rapid generation of the progeny cells with genomic instability in response to treatment stress leading to treatment resistance [15,16]. Aurora kinase A (AURKA) is one of the regulators of polyploidization to generate giant cells through mis-regulation of canonical G1–S–G2–M cell cycle without cell division followed by inactivation of TP53 [15–17]. Indeed, the ipC26 cells more highly expressed AURKA, but less phosphorylated TP53-ser15 (pTP53) than the scC26 cells (Fig. 3C), and were extremely resistant to 5-Fu treatment (Fig. 3D). These suggest i.p. tumors are polyploidy. The ipC26 cells were sensitive to an AURKA inhibitor MLN8237, but not a CDK4/6 inhibitor PD0332991 (Fig. 3D). When the ipC26 cells were s.c. implanted in mice, tumor growth was adversely promoted by 5-Fu treatment (P = 0.001 versus control), but not MLN treatment (Fig. 3E). CD11b$^+$PD1$^+$ cells were more seen in the ipC26

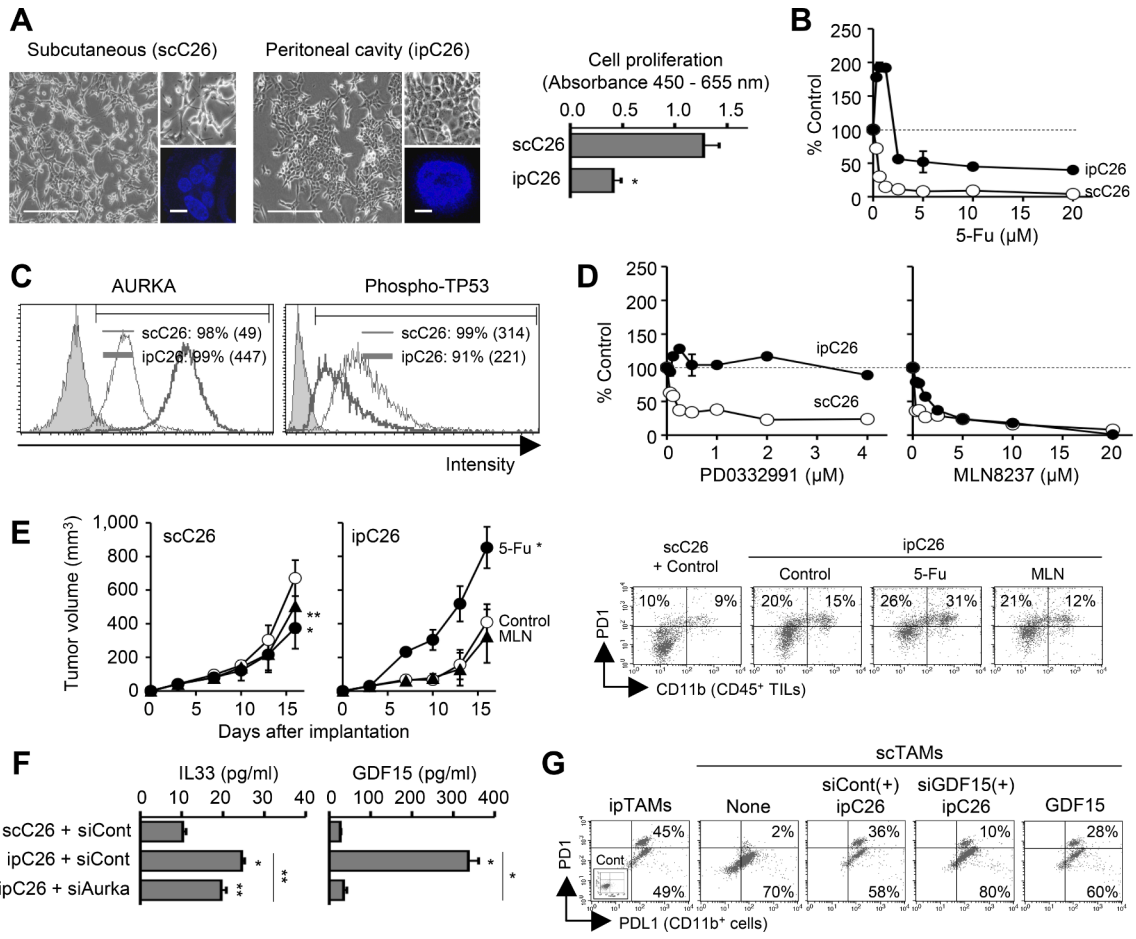

Fig. 3. AURKA is a determinant of chemoresistance of the i.p. tumor cells. (A) Low proliferative activity of the i.p. tumors with larger nuclei. Photos show more giant and adhesive appearance of the ipC26 cells (scale = 1000 μm) with large DAPI$^+$ nuclei (scale = 10 μm) as compared to that of the scC26 cells. (B) Chemoresistance of i.p. tumor cells. The scC26 cells (open circles) or ipC26 cells (closed circles) were cultured with 5-Fu for 2 days ($n = 3$). The graph depicts a percentage of the control cultured without agents (100%, dotted line). (C) Increase of AURKA expression, but decrease of phosphorylated TP53-ser15 (pTP53) expression in the ipC26 cells. Each MFI is indicated in a bracket. Shaded histogram, isotype control. (D) Blocking AURKA, but not CDK4/6, suppresses the ipC26 proliferation. The scC26 cells (open circles) or ipC26 cells (closed circles) were treated with a CDKI inhibitor PD0332991 or an AURKA inhibitor MLN8237 for 2 days ($n = 3$). The graph depicts a percentage of the control cultured without agents (100%, dotted line). (E) No aggravation of the ipC26 tumors after treatment with MLN8237. Mice were s.c. implanted with scC26 or ipC26 cells, and were i.p. injected with 5-Fu (20 mg/kg; closed circles), MLN8237 (5 mg/kg; closed triangles), or PBS (open circles) daily on days 3 - 7 ($n = 5$). TILs were analyzed for CD11b$^+$PD1$^+$ cells by flow cytometry on day 16. (F) Enhancement of IL33 and GDF15 release from the ipC26 cells. Tumor cells were transfected with AURKA-specific siRNA or control siRNA, and two days later, the re-cultured supernatants were tested for IL33 or GDF15 by ELISA ($n = 3$). (G) Induction of the PD1$^+$ subset in the CD11b$^+$ PECs by the ipC26-derived GDF15. The scTAMs were stimulated with tumor supernatants or GDF15 for 3 days, and were analyzed by flow cytometry. Graphs show means ± SDs. *$P < 0.01$, **$P < 0.05$ versus control. Representative data of three independent experiments.

tumors than the scC26 tumors, and were further expanded by 5-Fu treatment, but not MLN treatment (Fig. 3E). These suggest blocking AURKA prevents adverse progression of the polyploid i.p. tumors.

We previously identified IL33 as a critical molecule regulating cancer polyploidization by focusing on cancer stem cells and its bone marrow niche (bone metastasis) [18]. IL33 is an alarmin molecule that is released from some types of cells such as endothelial cells and fibroblasts in response to stress and damage, and is associated with diseases including allergy, infection, and cancer [19,20]. Indeed, the ipC26 cells more highly produced IL33 than the scC26 cells ($P = 0.002$), and the IL33 production was significantly suppressed by AURKA knockdown with the specific siRNA, while the effect was only slight (Figs. 3F and S1A). We then reviewed literature focusing on molecules with biological properties similar to those of IL33, and finally reached a member of the TGFβ superfamily GDF15, which has a lot of biological properties in common with IL33. GDF15 is associated with endothelial damage [21], cellular stress [22], and bone metastasis [23,24]. GDF15 was much more highly produced from the ipC26 cells than the scC26 cells ($P = 0.003$), and the GDF15 release from the ipC26 cells was abrogated by AURKA knockdown with the specific siRNA ($P = 0.004$), suggesting a close relationship between AURKA and GDF15 (Fig. 3F). Stimulation with recombinant GDF15 significantly reduced T-cell stimulatory activity of the scTAMs ($P = 0.033$; Fig. 2B). GDF15 knockdown in the ipC26 cells deprived of the CD11b$^+$PD1$^+$ cell-inducible activity (Fig. 3G), and conferred phagocytic activity (Fig. 2A) and T-cell stimulatory activity (Fig. 2B). These suggest AURKA$^+$ i.p. tumors generate impaired TAMs partly via the released GDF15.

Anti-tumor efficacy induced by MLN8237 therapy in the ascites models

We next evaluated MLN8237 therapeutic efficacy in the ascites models. MLN8237 therapy showed significant anti-tumor effects on tumor growth (i.p., $P = 0.007$; p.o., $P = 0.004$) and mouse survival (i.p., $P = 0.002$; p.o., $P = 0.030$) as compared to the control, and the i.p. treatment was more effective providing significantly better prognosis than the p.o. treatment ($P = 0.013$; Fig. 4A). In the mice, CD11b$^+$Gr1$^+$ cells almost disappeared in the PECs (Fig. 4B). The MLN8237 therapy synergized with anti-PD1 efficacy (tumor growth, $P = 0.002$; mouse

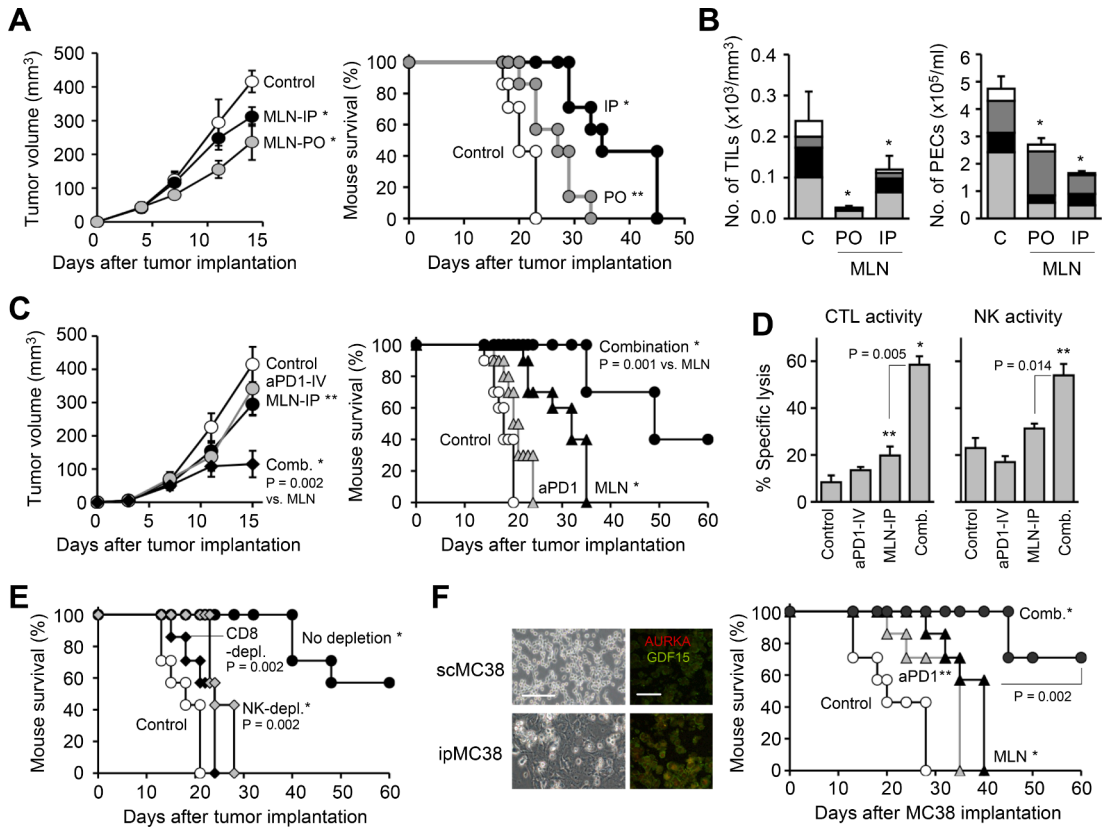

Fig. 4. Anti-tumor efficacy induced by MLN8237 therapy in the ascites models. (A, B) MLN8237 therapy is effective in mice with ascites. The ascites models were i.p. (IP; closed circles) or orally (p.o. or PO; gray circles) administered with MLN8237 (MLN, 5 mg/kg) or PBS (open circles) daily on days 3 - 6 after tumor implantation ($n = 7$). Tumor growth and mouse survival were observed (A), and TILs and PECs were analyzed by flow cytometry on day 15 after tumor implantation (B). Light gray, $CD3^+CD4^+$ T cells. Closed, $CD3^+CD8^+$ T cells. Dark gray, $DX5^+$ NK cells. Open, $CD11b^+Gr1^+$ myeloid cells. (C, D) MLN8237 therapy synergizes with anti-PD1 in treatment of mice with ascites. The ascites models were i.p. injected with MNL or PBS daily on days 3 - 5, and/or were i.v. injected with anti-PD1 mAb or mIgG on days 5 and 8 ($n = 10$). Open circles, control. Closed triangles, MLN. Gray triangles, anti-PD1 mAb. Closed circles, MLN + anti-PD1 mAb. Tumor growth and mouse survival were observed (C), and splenic $CD8^+$ T cells (target = Colon26) and NK cells (target = Yac-1) of the mice were tested for tumor killing activity on day 15 (ET ratio = 20:1; $n = 5$). (E) Requirement of both $CD8^+$ T cells and NK cells for the anti-tumor efficacy induced by the MLN/aPD1 combination therapy. The mice were i.p. injected with anti-CD8 (closed diamonds), anti-asialo GM1 antibody (gray diamonds), or PBS (no depletion; closed circles) during the combination therapy ($n = 7$). Open circles, untreated control. (F) Anti-tumor efficacy induced by the MLN/aPD1 combination therapy in another CRC models. C57BL/6 mice were s.c. and i.p. implanted with murine CRC MC38 cells, and were treated with MLN and/or anti-PD1 mAb ($n = 7$). Tumor cells were isolated from the s.c. tumor tissues (scMC38) or PECs (ipMC38) of the mice 2 weeks after tumor implantation. Scale, 1000 μm. Graphs show means ± SDs. $^*P < 0.01$, $^{**}P < 0.05$ versus control. Representative data of three independent experiments.

survival, $P = 0.001$) as compared to the monotherapy (Fig. 4C), and induced CTLs and NK cells having significantly higher cytotoxity in the mice (Fig. 4D). The therapeutic efficacy was abrogated by depletion of $CD8^+$ T cells and NK cells, suggesting requirement of both cells (Fig. 4E). To validate generality of the findings, we treated different tumor models that C57BL/6 mice were s.c. and i.p. implanted with murine CRC MC38 cells. The combination regimen was also significantly effective in this model ($P = 0.002$; Fig. 4F). MC38 cells isolated from the PECs were also giant expressing AURKA and GDF15. These suggest blocking AURKA is effective in treatment of hosts with i.p. tumors, and greatly contributes to anti-PD1 therapy by successfully eliciting potent anti-tumor immunity.

Clinical relevancy of the AURKA-GDF15 axis

To further validate the findings in human system, we used xenograft models that immunodeficient nu/nu mice were s.c. and i.p. implanted with human CRC HCT116 cells. Tumor cells obtained from the PECs (ipHCT116) were giant with larger nuclei, and showed significantly lower proliferative ability than tumor cells obtained from s.c. tumors (scHCT116; Fig. 5A). The ipHCT116 cells highly expressed AURKA, but less pTP53, than the scHCT116 cells (Fig. 5B). Blocking AURKA significantly suppressed cell proliferation (Fig. 5C) and GDF15 production (Figs. 5D and S1B). When human CTLs were stimulated with the ipHCT116 supernatant, cell proliferation was significantly suppressed ($P = 0.004$ versus scHCT116), but was saved by GDF15 knockdown in the ipHCT116 cells ($P = 0.027$ versus control; Figs. 5E and S1B). These were consistent with the results observed in the mouse system.

We also analyzed PECs isolated from peritoneal lavage fluids of gastric cancer patients by flow cytometry ($n = 16$; Table S1). Tumor cells were giant with a large nucleus, and $CD11b^+PD1^+$ TAMs were significantly increased in the PECs with tumors compared to the PECs without tumors ($P = 0.0047$; Fig. 6A and B). The $CD11b^+PD1^+$ TAM increase was significantly correlated with increase of T cells expressing multiple IC molecules ($P < 0.0083$; Fig. 6C). These suggest expansion of the $CD11b^+PD1^+$ TAMs is a possible surrogate marker of i.p. tumor dissemination accompanied by immune exhaustion in patients. Targeting AURKA may be a promising strategy for treating GI patients with i.p. tumors.

Discussion

In this study, we identified AURKA as a key determinant of refractory i.p. tumors. AURKA expression in the i.p. tumors regulates treatment

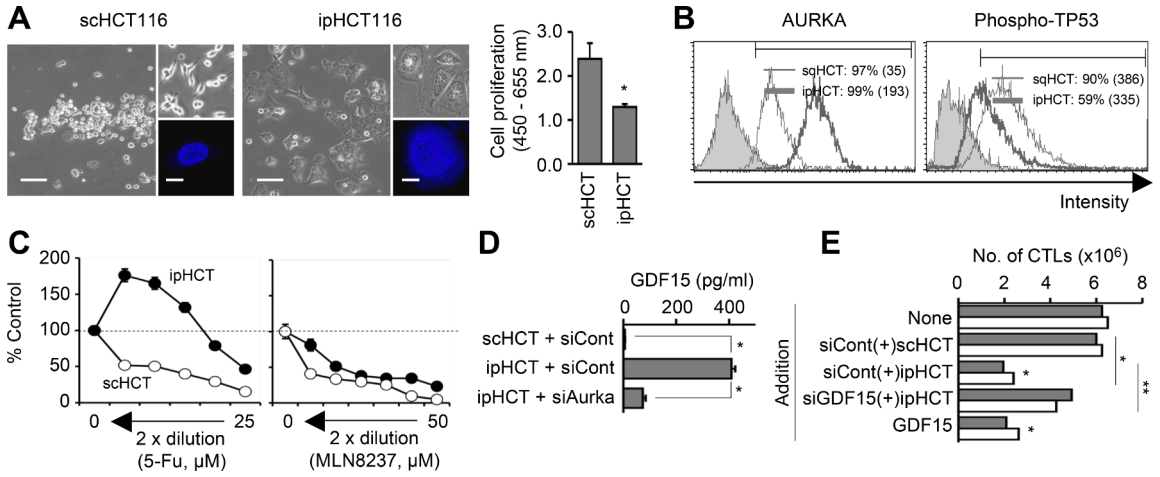

Fig. 5. Significance of the AURKA-GDF15 axis in human system. (A) Morphological and functional changes of human CRC HCT116 cells within the peritoneal cavity of immunodeficient nu/nu mice. Tumor cells were isolated from the s.c. tumor tissues (scHCT116) or PECs (ipHCT116) 2 weeks after tumor implantation (n = 3). Photos show more giant and adhesive appearance of the ipHCT116 cells (scale = 1000 μm) with large DAPI$^+$ nuclei (scale = 10 μm) as compared to that of the scHCT116 cells. (B) Increase of AURKA expression, but decrease of pTP53 expression in the ipHCT116 cells. Each MFI is indicated in a bracket. Shaded histogram, isotype control. (C) Blocking AURKA suppresses the ipHCT116 proliferation. The scHCT116 cells (open circles) or ipHCT116 cells (closed circles) were treated with 5-Fu or MLN8237 for 2 days (n = 3). The graph depicts a percentage of the control cultured without agents (100%, dotted line). (D) Enhancement of GDF15 release from the ipHCT116 cells possibly via AURKA. The cultured supernatants of the siRNA-transfected tumor cells were tested by ELISA (n = 3). (E) CTL induction is suppressed by the ipHCT116-derived GDF15. Tumor antigen SAGE-specific CTLs were established using PBMCs obtained from two donors (closed and open bars), and were cultured with SAGE peptides and IL2 in the presence of the tumor supernatants (5 x dilution) or GDF15 (20 ng/ml) for 5 days (n = 3). Graphs show means ± SDs. *P < 0.01, **P < 0.05 versus control. Representative data of three independent experiments.

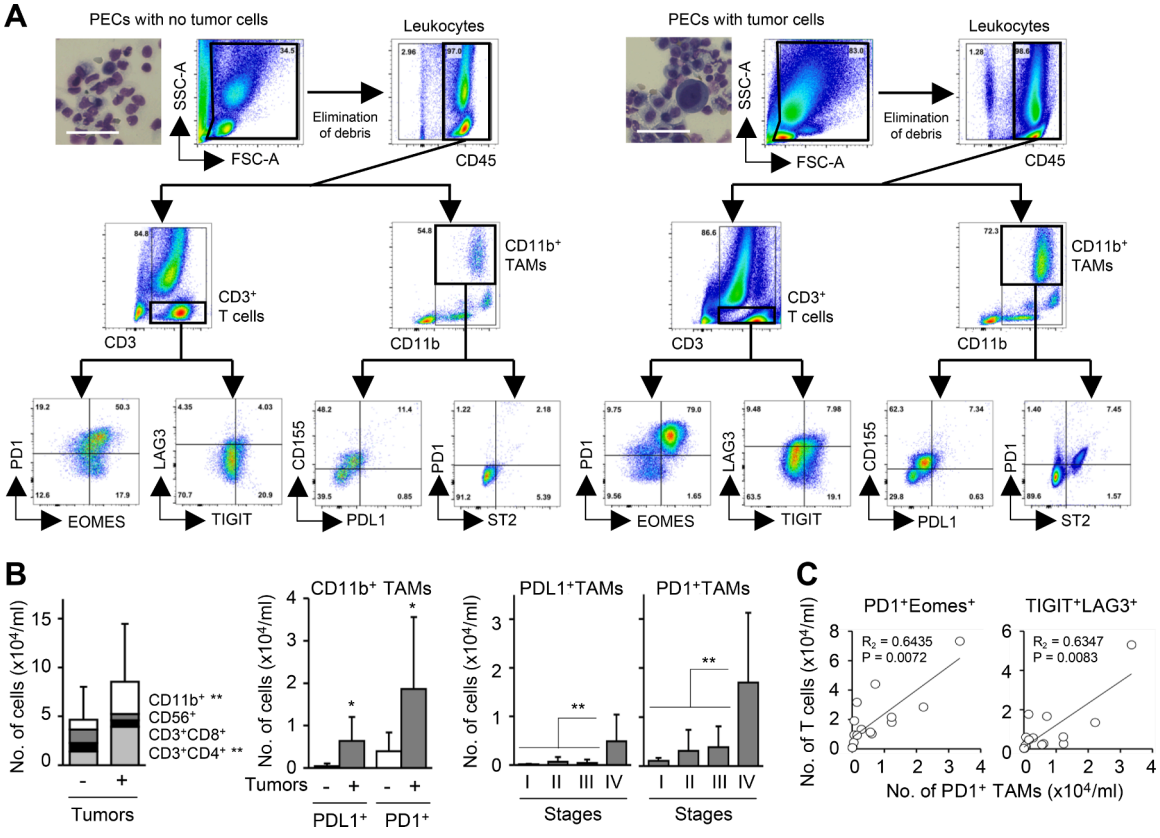

Fig. 6. The CD11b$^+$PD1$^+$ TAMs are expanded in PECs of gastric cancer patients. (A) Gating strategy to analyze CD11b$^+$ TAMs and CD3$^+$ T cells in human PECs by flow cytometry. The peritoneal lavage fluids were obtained from gastric cancer patients at initiation of surgical tumor resection (stage I x 2, stage II x 5, stage III x 5, and stage IV x 4; n = 16). Photos show HE-stained PECs (scale = 50 μm). (B) CD11b$^+$PD1$^+$ cells are significantly expanded in PECs particularly with tumor cells (n = 3) as compared to PECs without tumor cells (n = 13). Light gray, CD3$^+$CD4$^+$ T cells. Closed, CD3$^+$CD8$^+$ T cells. Dark gray, DX5$^+$ NK cells. Open, CD11b$^+$ TAMs. *P < 0.01, **P < 0.05 versus PECs without tumor cells. (C) Significant correlation between increase of the CD11b$^+$PD1$^+$ TAMs and increase of potentially exhausted CD3$^+$ T cells expressing multiple immune checkpoint molecules. Graphs show means ± SDs.

resistance not only via tumor polyploidization, but also via expansion of impaired TAMs through GDF15 production. Some studies have also shown regulation of production of cytokines and chemokines by AURKA [25,26], although AURKA is a protein kinase mainly regulating cell cycle. However, locking AURKA with MLN8237 or siRNAs abrogates these adverse events, and successfully elicits anti-tumor immunity in the ascites models. The $CD11b^{+}PD1^{+}$ TAMs are also expanded in the PECs particularly along with tumor cells in gastric cancer patients. Thus, MLN8237 therapy may be useful for treating GI cancer patients with i.p. tumors. Many AURKA inhibitors have been clinically developed, while most trials failed due to the serious toxicity [27,28]. However, i.p. injection may be an alternative but encouraging way to give less systemic side effects, but higher cytotoxity to the local peritoneal cavity where to have high risk of tumor spread.

EMT has been considered as a biological process crucial for i.p. tumor dissemination [5,6]. However, it should be noted that EMT is only a part of the metastatic cascade. The disseminated dormant tumor cells must reawaken to grow in the secondary site, possibly through the reverse process of EMT and/or polyploidy. Particularly, cancer polyploidy is a principal program in cancer stemness to massively increase intratumoral heterogeneity and complexity by generating numerous progeny cells in response to treatment stress [15–17]. Incidence and frequency of polyploid tumor cells are clinically associated with the grade, chemoresistance, and poor prognosis of cancer patients [29,30]. AURKA expression in the i.p. tumor cells could be induced by endoreplication in response to hypoxia in the peritoneal cavity, because hypoxia is a critical trigger of cancer polyploidization [15–17]. Interaction with peritoneal immune cells may be also involved in the mechanism of AURKA upregulation in the i.p. tumor cells.

We previously identified IL33 as a key driver of cancer progression [18]. IL33 induces both tumor polyploidization and immunosuppression mediated by various immunosuppressive $ST2^{+}$ cells, including mast cells, myeloid-derived suppressor cells (MDSCs), and regulatory T cells (Tregs). In the PECs of gastric cancer patients, the $CD11b^{+}PD1^{+}$ TAMs highly expressed ST2 (Fig. 6A). The IL33-ST2 axis may be also involved in the mechanisms of the i.p. tumor progression. Recent studies have revealed the landscape of i.p. immunity mediated by not only inflammatory macrophages [9], but also immunosuppressive cells, such as MDSCs [31] and Tregs [32]. IL33 and GDF15 might be, at least partly, underlying the identified mechanisms. PD1 expression in myeloid cells and the close relationship with poor prognosis have been demonstrated in mice and human [33,34]. These studies demonstrated PD1 knockout or blockade in the cells abrogates the immunosuppressive activity, and induces potent anti-tumor immunity in mouse tumor models [35–37]. However, in our study, the impact of blocking PD1/PDL1 was small in both *in vitro* and *in vivo* settings. This discrepancy might be come from the experimental conditions, particularly of tumor models with i.p. tumors. A variety of agents have been evaluated in combination with anti-PD1/PDL1 therapy in numerous clinical trials [38]. However, the optimization is still underway. Blocking AURKA may be a strong candidate particularly in the treatment of GI cancer.

This study provides a rationale of targeting AURKA in the treatment of GI cancer patients, particularly with disseminated i.p. tumors. As therapeutic strategy, blocking AURKA may be useful for suppressing i.p. tumor progression. As diagnostic strategy, monitoring the increased $CD11b^{+}PD1^{+}$ TAMs (those are possibly expanded by $AURKA^{+}$ tumors) in the lavage fluids at surgery may be useful for prediction of the onset of i.p. tumor progression as a surrogate marker of i.p. tumors hiding somewhere within the peritoneal cavity of the GI cancer patients, although only tumor cells are monitored in the present cytological diagnosis. A larger scale study using more clinical samples is needed for the validation.

CRediT authorship contribution statement

Hiroki Ozawa: Investigation, Formal analysis, Writing – original draft. **Hiroshi Imazeki:** Investigation, Formal analysis. **Yamato Ogiwara:** Investigation, Formal analysis. **Hirofumi Kawakubo:** Data curation. **Kazumasa Fukuda:** Investigation. **Yuko Kitagawa:** Supervision. **Chie Kudo-Saito:** Conceptualization, Investigation, Formal analysis, Writing – original draft.

Declaration of Competing Interest

The authors have no competing financial interests.

Founding sources

This study was partly supported by the Japan Agency for Medical Research and Development P-CREATE, Tokyo, Japan (Grant Number 106209).

Supplementary materials

Supplementary material associated with this article can be found, in the online version, at doi:10.1016/j.tranon.2021.101307.

References

[1] N. Fang, H.Q. Zhang, B. He, M. Xie, S. Lu, Y.Y. Wan, et al., Clinicopathological characteristics and prognosis of gastric cancer with malignant ascites, Tumour Biol. 35 (2014) 3261–3268, https://doi.org/10.1007/s13277-013-1426-3.
[2] Z. Wang, J.Q. Chen, J.L. Liu, L. Tian, Issues on peritoneal metastasis of gastric cancer: an update, World J. Surg. Oncol. 17 (2019) 215, https://doi.org/10.1186/s12957-019-1761-y.
[3] A.C. Gamboa, J.H. Winer, Cytoreductive surgery and hyperthermic intraperitoneal chemotherapy for gastric cancer, Cancers (Basel) 11 (2019) 1662, https://doi.org/10.3390/cancers11111662.
[4] D.K.A. Chia, J.B.Y. So, Recent advances in intra-peritoneal chemotherapy for gastric cancer, J. Gastric Cancer 20 (2020) 115–126, https://doi.org/10.5230/jgc.2020.20.e15.
[5] F. Sun, M. Feng, W. Guan, Mechanisms of peritoneal dissemination in gastric cancer, Oncol. Lett. 14 (2017) 6991–6998, https://doi.org/10.3892/ol.2017.7149.
[6] Y. Chen, Q. Zhou, H. Wang, W. Zhuo, Y. Ding, J. Lu, et al., Predicting peritoneal dissemination of gastric cancer in the era of precision medicine: molecular characterization and biomarkers, Cancers (Basel) 12 (2020) 2236, https://doi.org/10.3390/cancers12082236.
[7] K. Stoletov, P.H. Beatty, J.D. Lewis, Novel therapeutic targets for cancer metastasis, Expert Rev. Anticancer Ther. 20 (2020) 97–109, https://doi.org/10.1080/14737140.2020.1718496.
[8] C. Kudo-Saito, Y. Ozaki, H. Imazeki, H. Hayashi, J. Masuda, H. Ozawa, et al., Targeting oncoimmune drivers of cancer metastasis, Cancers (Basel) 13 (2021) 554, https://doi.org/10.3390/cancers13030554.
[9] H. Song, T. Wang, L. Tian, S. Bai, L. Chen, Y. Zuo, et al., Macrophages on the peritoneum are involved in gastric cancer peritoneal metastasis, J. Cancer 10 (2019) 5377–5387, https://doi.org/10.7150/jca.31787.
[10] S. Shalapour, M. Karin, Immunity, inflammation, and cancer: an eternal fight between good and evil, J. Clin. Invest. 125 (2015) 3347–3355, https://doi.org/10.1172/JCI80007.
[11] K.E. Pauken, E.J. Wherry, Overcoming T cell exhaustion in infection and cancer, Trends Immunol. 36 (2015) 265–276, https://doi.org/10.1016/j.it.2015.02.008.
[12] M.J. Overman, S. Lonardi, K.Y.M. Wong, H.J. Lenz, F. Gelsomino, M. Aglietta, et al., Durable clinical benefit with nivolumab plus ipilimumab in DNA mismatch repair-deficient/microsatellite instability-high metastatic colorectal cancer, J. Clin. Oncol. 36 (2018) 773–779, https://doi.org/10.1200/JCO.2017.76.9901.
[13] J.J. Havel, D. Chowell, T.A. Chan, The evolving landscape of biomarkers for checkpoint inhibitor immunotherapy, Nat. Rev. Cancer 19 (2019) 133–150, https://doi.org/10.1038/s41568-019-0116-x.
[14] C. Kudo-Saito, M. Yura, R. Yamamoto, Y. Kawakami, Induction of immunoregulatory CD271+ cells by metastatic tumor cells that express human endogenous retrovirus H, Cancer Res. 74 (2014) 1361–1370, https://doi.org/10.1158/0008-5472.CAN-13-1349.
[15] J. Coward, A. Harding, Size does matter: why polyploid tumor cells are critical drug targets in the war on cancer, Front. Oncol. 4 (2014) 123, https://doi.org/10.3389/fonc.2014.00123.
[16] S. Zhang, I. Mercado-Uribe, Z. Xing, B. Sun, J. Kuang, J. Liu, Generation of cancer stem-like cells through the formation of polyploid giant cancer cells, Oncogene 33 (2014) 116–128, https://doi.org/10.1038/onc.2013.96.
[17] S.R. Amend, G. Torga, K.C. Lin, L.G. Kostecka, A. de Marzo, R.H. Austin, et al., Polyploid giant cancer cells: unrecognized actuators of tumorigenesis, metastasis, and resistance, Prostate 79 (2019) 1489–1497, https://doi.org/10.1002/pros.23877.
[18] C. Kudo-Saito, T. Miyamoto, H. Imazeki, H. Shoji, K. Aoki, N. Boku, IL33 is a key driver of treatment resistance of cancer, Cancer Res. 80 (2020) 1981–1990, https://doi.org/10.1158/0008-5472.CAN-19-2235.

[19] F.Y. Liew, J.P. Girard, H.R. Turnquist, Interleukin-33 in health and disease, Nat. Rev. Immunol. 16 (2016) 676–689, https://doi.org/10.1038/nri.2016.95.
[20] B. Griesenauer, S. Paczesny, The ST2/IL-33 axis in immune cells during inflammatory diseases, Front. Immunol. 8 (2017) 475, https://doi.org/10.3389/fimmu.2017.00475.
[21] L. Rochette, M. Zeller, Y. Cottin, C. Vergely, Insights into mechanisms of GDF15 and receptor GFRAL: therapeutic targets, Trends Endocrinol. Metab. 31 (2020) 939–951, https://doi.org/10.1016/j.tem.2020.10.004.
[22] P.J. Emmerson, K.L. Duffin, S. Chintharlapalli, X. Wu, GDF15 and growth control, Front. Physiol. 9 (2018) 1712, https://doi.org/10.3389/fphys.2018.01712.
[23] J. Windrichova, R. Fuchsova, R. Kucera, O. Topolcan, O. Fiala, J. Finek, et al., MIC1/GDF15 as a bone metastatic disease biomarker, Anticancer Res. 37 (2017) 1501–1505, https://doi.org/10.21873/anticanres.11477.
[24] A. Spanopoulou, V. Gkretsi, Growth differentiation factor 15 (GDF15) in cancer cell metastasis: from the cells to the patients, Clin. Exp. Metastasis 37 (2020) 451–464, https://doi.org/10.1007/s10585-020-10041-3.
[25] C.C. Yen, S.C. Chen, G.Y. Hung, P.K. Wu, W.Y. Chua, Y.C. Lin, et al., Expression profiledriven discovery of AURKA as a treatment target for liposarcoma, Int. J. Oncol. 55 (2019) 938–948, https://doi.org/10.3892/ijo.2019.4861.
[26] J. Wang, T. Hu, Q. Wang, R. Chen, Y. Xie, H. Chang, et al., Repression of the AURKA-CXCL5 axis induces autophagic cell death and promotes radiosensitivity in non-small-cell lung cancer, Cancer Lett. 509 (2021) 89–104, https://doi.org/10.1016/j.canlet.2021.03.028.
[27] V. Bavetsias, S. Linardopoulos, Aurora kinase inhibitors: current status and outlook, Front. Oncol. 5 (2015) 278, https://doi.org/10.3389/fonc.2015.00278.
[28] A. Tang, K. Gao, L. Chu, R. Zhang, J. Yang, J. Zheng, Aurora kinases: novel therapy targets in cancers, Oncotarget 8 (2017) 23937–23954, https://doi.org/10.18632/oncotarget.14893.
[29] F. Fei, D. Zhang, Z. Yang, S. Wang, X. Wang, Z. Wu, et al., The number of polyploid giant cancer cells and epithelial-mesenchymal transition-related proteins are associated with invasion and metastasis in human breast cancer, J. Exp. Clin. Cancer Res. 34 (2015) 158, https://doi.org/10.1186/s13046-015-0277-8.
[30] B. Xuan, D. Ghosh, E.M. Cheney, E.M. Clifton, M.R Dawson, Dysregulation in actin cytoskeletal organization drives increased stiffness and migratory persistence in polyploidal giant cancer cells, Sci. Rep. 8 (2018) 11935, https://doi.org/10.1038/s41598-018-29817-5.
[31] Y. Sugita, K. Yamashita, M. Fujita, M. Saito, K. Yamada, K. Agawa, et al., CD244(+) polymorphonuclear myeloidderived suppressor cells reflect the status of peritoneal dissemination in a colon cancer mouse model, Oncol. Rep. 45 (2021) 106, https://doi.org/10.3892/or.2021.8057.
[32] I. Wertel, J. Surowka, G. Polak, B. Barczynski, W. Bednarek, J. Jakubowicz-Gil, et al., Macrophage-derived chemokine CCL22 and regulatory T cells in ovarian cancer patients, Tumour Biol. 36 (2015) 4811–4817, https://doi.org/10.1007/s13277-015-3133-8.
[33] D. Lu, Z. Ni, X. Liu, S. Feng, X. Dong, X. Shi, et al., Beyond T Cells: understanding the role of PD-1/PD-L1 in tumor-associated macrophages, J. Immunol. Res. 2019 (2019), 1919082, https://doi.org/10.1155/2019/1919082.
[34] Y. Kono, H. Saito, W. Miyauchi, S. Shimizu, Y. Murakami, Y. Shishido, et al., Increased PD-1-positive macrophages in the tissue of gastric cancer are closely associated with poor prognosis in gastric cancer patients, BMC Cancer 20 (2020) 175, https://doi.org/10.1186/s12885-020-6629-6.
[35] T.S. Lim, V. Chew, J.L. Sieow, S. Goh, J.P. Yeong, A.L. Soon, et al., PD-1 expression on dendritic cells suppresses CD8(+) T cell function and antitumor immunity, Oncoimmunology 5 (2016), e1085146, https://doi.org/10.1080/2162402X.2015.1085146.
[36] S.R. Gordon, R.L. Maute, B.W. Dulken, G. Hutter, B.M. George, M.N. McCracken, et al., PD-1 expression by tumour-associated macrophages inhibits phagocytosis and tumour immunity, Nature 545 (2017) 495–499, https://doi.org/10.1038/nature22396.
[37] P. Dhupkar, N. Gordon, J. Stewart, E.S. Kleinerman, Anti-PD-1 therapy redirects macrophages from an M2 to an M1 phenotype inducing regression of OS lung metastases, Cancer Med. 7 (2018) 2654–2664, https://doi.org/10.1002/cam4.1518.
[38] J. Xin Yu, V.M. Hubbard-Lucey, J Tang, Immuno-oncology drug development goes global, Nat. Rev. Drug Discov. 18 (2019) 899–900, https://doi.org/10.1038/d41573-019-00167-9.